

A Thin-Film Flexible Defect-Mode Laser

Taimoor Ali, Jia-De Lin, Benjamin Snow, Xiuze Wang, Steve J. Elston and Stephen M. Morris**

Taimoor Ali, Dr. Jia-De Lin, Xiuze Wang, Prof. Steve J. Elston, Dr. Stephen M. Morris
Department of Engineering Science, University of Oxford, Parks Road, Oxford, OX1 3PJ, UK
E-mail: taimoor.ali@eng.ox.ac.uk, stephen.morris@eng.ox.ac.uk

Dr. Benjamin Snow
Merck Chemicals Ltd., Chilworth Technical Center, University Parkway, Southampton, SO16 7QD, UK

Keywords: thin-film laser, liquid crystal, defect-mode, flexible laser

This communication demonstrates laser emission from a flexible defect-mode structure consisting of two photopolymerized liquid crystal thin films separated by a dye-doped polymethylmethacrylate defect layer. A simple and cost-effective film transfer technique is used to fabricate the flexible laser and results are presented on the corresponding laser emission characteristics, which shows single-mode laser emission at $\lambda = 582$ nm, with an excitation threshold of $E_{th} = 12.3 \pm 0.5 \mu\text{J}/\text{cm}^2/\text{pulse}$ and a slope efficiency of $\eta_s = 6.0 \pm 0.3\%$. Results are also presented on the polarization state of the laser emission and this is compared with the findings reported in the literature. Finally, laser beam steering is demonstrated up to 42° by subjecting the device to a mechanically-induced deformation that creates a radius of curvature of 5 mm, which is of potential interest for conformable and wearable technology platforms.

Thin-film laser devices consisting of organic materials that can be fabricated using solution processing techniques such as roll-to-roll, spin-coating and printing^[1,2] are naturally suited to flexible platforms. Feedback in these lasers can be achieved in a variety of ways, but those that naturally form periodic photonic structures, such as chiral nematic (cholesteric) liquid crystals (CLC) are particularly desirable as they can simplify the fabrication process.^[3–5] Towards this end, flexible laser devices consisting of dye-doped CLCs have been

demonstrated previously for band-edge laser emission, whereby the gain medium is dispersed directly into the host material and laser emission is observed at one edge of the reflection band (photonic band gap)^[6]. However, a disadvantage of this configuration is that to form a rugged but flexible band-edge laser device, the dye-doped CLC film is typically photopolymerized using ultraviolet light, which can cause unwanted photo-bleaching of the dye (gain) molecules that negatively affects the performance of the laser^[7].

An alternative device configuration that circumvents the potential issue of photo-bleaching of the gain medium when the CLC is photopolymerized is **the defect-mode structure**^[8–12]. In this configuration a separate layer is formed for the gain medium that is sandwiched between two CLC layers (**Figure 1**). This structure creates a defect in the macroscopic helical structure and therefore a leaky mode within the band-gap^[13–17]. Furthermore, as the gain medium is de-coupled from the CLC the device architecture allows for a wide variety of emissive compounds to be used that would not otherwise be soluble in the CLC host^[18,19].

Here, we demonstrate a flexible defect-mode LC laser. Figure 1a illustrates the processing steps required to form the flexible defect-mode laser (see Experimental Section). In summary, the resulting stack consists of a flexible substrate, a polymerizable CLC, a PMMA barrier layer, a dye-doped PMMA defect layer, another PMMA barrier layer followed by the top CLC layer and flexible substrate. The total thickness of the defect layer is 720 nm. Figure 1b shows examples of the optical polarization microscope images recorded of the sample when viewed in reflection at a magnification of 10× with a halogen white light source. Two images are presented: the first (Figure 1bi) shows an example microscope image of the photo-polymerized CLC film after filling into the glass cell and before it is transferred to the flexible substrate while the second microscope image (Figure 1bii) shows the optical texture

after assembling the complete device stack comprising flexible substrate/CLC/PMMA/dye-doped PMMA/PMMA/CLC/flexible substrate. Encouragingly, a uniform (single color) optical texture is observed in both images, indicating that the pitch is uniform over areas of at least $700\text{ }\mu\text{m} \times 700\text{ }\mu\text{m}$, which is significantly larger than the pump spot size of the Nd:YAG laser that is used to excite the thin-film laser device. Furthermore, the images confirm that the monodomain texture is retained after the CLC film is transferred onto the flexible substrate and after the addition of the barrier and defect layers. It should be noted that spacer beads are present in Figure 1bii, which implies that these are also transferred when the CLC film is delaminated from the glass substrate and attached to the flexible substrate.

To confirm that the CLC reflectors remain intact after device fabrication, Figure 1c presents results of the reflection spectrum of the CLC film after polymerization, but before the top glass substrate is removed, along with the reflection spectra from the top and bottom CLC layers after the device has been assembled. The center of the band-gap of the photo-polymerized CLC is found to be located initially at $\lambda_c = 615\text{ nm}$, which is then blue-shifted to $\lambda_c = 595 \pm 5\text{ nm}$ after device construction. This relatively small shift in the band-gap is likely to be due to a slight contraction of the pitch of the helix during the removal of the anisole, which causes a deswelling of the CLC films as excess solvent, which is present during the capillary filling stage, is removed. It can also be seen that the position and overall shape of the reflection band for the top and bottom CLC layers are almost identical, indicating that the pitch is uniform throughout the device.

It is understood that within the band-gap the Density of Photon States (DoS) is zero for the circular polarization sense that matches the handedness of the helix^[20]. However, when a discontinuity is introduced within the helical structure, either by introducing an isotropic/anisotropic layer or by introducing a phase slip, a leaky (defect) mode is created^[21].

By overlapping the emission spectrum of the gain medium with the defect-mode(s), laser emission can be observed when optically excited at excitation fluences that exceed the laser threshold. From measurements of the transmission of the complete device stack, it is often difficult to discern the presence of the defect-mode as it is regularly the case that the spectral width of the defect-mode is very narrow and beyond the resolution of the spectrometer used to record the transmission spectrum of the band-gap. In our work, the spectrometer has a resolution of 1.5 nm; however, the defect-mode is likely to have a width of no more than 0.04 nm as noted in previous reports^[19] and is in accordance with our simulations using the 4×4 Berreman matrix. Nevertheless, we believe that a defect-mode is present as evidenced from the laser emission characteristics.

When the sample is optically excited with an Nd:YAG laser (see Experimental section and **Figure S1**) with fluences that are below the excitation threshold, for example at 5.60 $\mu\text{J}/\text{cm}^2/\text{pulse}$ and 7.55 $\mu\text{J}/\text{cm}^2/\text{pulse}$, a broad fluorescence spectrum can be observed, corresponding to the fluorescence spectrum of the laser dye PM597 (see **Figure S2 – a & b** in the Supplementary Information). However, when the optical excitation is increased above the excitation threshold fluence, it was found that the flexible device generated single mode laser emission centered at $\lambda_{\text{LC}} = 582$ nm. **Figure 2a** shows the spectrum of the laser emission alongside the relative position of the reflection band of the CLC layers, where it can be seen that the laser emission is observed to occur within the band-gap, consistent with a defect-mode. However, when the higher excitation fluence is increased, i.e., to 24 $\mu\text{J}/\text{cm}^2/\text{pulse}$, the fluorescent pedestal can only be seen when the laser spectrum is enlarged around the low emission intensities (see **Figure S2-c** in the Supplementary Information). This is also supported by results obtained for the transmission spectrum of the complete device stack using a 4×4 Berreman matrix approach. The simulation shows that a defect-mode occurs at λ

= 582 nm, which is consistent with our results for the laser emission wavelength. It is, therefore, considered that the laser emission is the result of the presence of a defect-mode within the band-gap.

Figure 2b illustrates the evolution of the laser emission spectrum as the excitation fluence is increased, highlighting the appearance of a laser emission line centered at $\lambda = 582$ nm, which grows in magnitude with the excitation fluence. An example of the input-output characteristics for the laser is shown in Figure 2c which shows a discontinuity in the gradient, corresponding to the excitation threshold, at $E_{th} = 12.3 \pm 0.5 \mu\text{J}/\text{cm}^2/\text{pulse}$. The slope efficiency of the laser was determined to be approximately $6.0 \pm 0.3\%$ while the divergence of the flexible laser was found to be $8.8^\circ \pm 1^\circ$ when the pump energy was set to $E = 340 \text{ nJ} \pm 10 \text{ nJ}$. Previous reports indicate that the divergence of band-edge CLC lasers varies from a few degrees to tens of degrees and is found to depend on parameters such as the pump energy, CLC film thickness and boundary conditions of the active layer^[22]. Our results presented here reveal a divergence angle that is comparable in magnitude.

The spectral position of the defect-mode can be controlled by changing the thickness of the defect layer and this is shown in the results from simulations using the 4×4 Berreman matrix approach (see **Figure S3** in the Supplementary Information). In this example, the thickness of the defect layer is varied from 260 nm to 460 nm and is found to result in a single mode within the band gap that varies from 575 nm to 625 nm, respectively. The change in the wavelength of the defect-mode could, in principle, be used to demonstrate wavelength tuning by adjusting the defect layer thickness. However, we do not consider this here, as our fabrication technique does not currently allow for the precise control of the thickness of the defect and thus the position of the resonant mode.

The threshold fluence presented here is low compared to previously reported LC band-edge/defect-mode laser and deserves further comment^[23–31]. In the literature, the excitation threshold of LC defect-mode lasers is typically found to lie within the range of hundreds of $\mu\text{J}/\text{cm}^2/\text{pulse}$ to tens of $\text{mJ}/\text{cm}^2/\text{pulse}$ ^[23–26], whereas the lowest laser threshold reported for band-edge LC lasers is of the order of a few $\text{mJ}/\text{cm}^2/\text{pulse}$ ^[27–29]. The lower threshold observed for defect mode lasers is generally understood to result from the higher density of states at the defect-mode compared to that of the modes located at the band-edges^[32]. Even though our threshold value is on the lower end of the regime for other reported defect-mode lasers it is not out of line with other organic thin film lasers that have reported excitation fluences as low as a few tens of $\text{nJ}/\text{cm}^2/\text{pulse}$ ^[30]. For the flexible device presented here, the low threshold is believed to be due to a combination of the high quantum efficiency ($>70\%$) of the laser dye^[33] and the confinement of the gain medium to the defect layer, which avoids the photobleaching of the dye when the gain medium is dispersed within the CLC mixture^[24–26]. The polarization of the laser emission from the flexible device was determined using the optical setup in **Figure S4**. Figure 2d reveals a dominant RCP component with a small amount of LCP light. For an isotropic defect layer, which is the configuration used here, previous research has shown that the polarization of the mode is typically observed to be circularly polarized of the same handedness as that of the CLC helix^[34–36]. Our results are in broad agreement in that we see a dominant RCP component in accordance with the right-handed helix of our CLC layers.

To demonstrate the flexibility of our device, **Figure 3** presents results of the variation in the emission direction when the device was subjected to a mechanical deformation. **For this experiment, the pump beam from the Nd:YAG laser was scanned across the device so as to illuminate different active regions in the thin film laser when it was mechanically deformed.** Figure 3b shows a schematic illustrating the concept of the experiment where, in this case, the flexible laser device was pumped at five separate active locations, labelled I to V

in the figure, across the thin film. In accordance with the deformation of the thin film and thus the different orientations of the helix axis, this resulted in LC laser emission at different locations on the illumination screen, shown with the corresponding Roman numerals. A photograph of the flexible laser when it is held in a curved configuration and optically excited by the Nd:YAG laser is shown in Figure 3c(i), where the corresponding LC laser emission (red light) and the pump laser (at the center) can be seen illuminating the screen. The following set of images in Figures 3c (ii-vi) show the beam steering phenomena of the flexible laser device.

In Figure 3c (ii), optical pumping at the center of the device corresponds to location I and therefore both the pump spot and LC laser emission are observed on the viewing screen. The angle (θ) represents the angle between the propagation direction of the pump beam and the normal to the surface of the thin-film. At the central location (labelled as I), the normal to the substrate of the thin film laser is parallel to the propagation direction of the pump and therefore $\theta = 0^\circ$. Since the helix axis in the CLC layers is oriented along the normal to the substrates this means that the helix axis and the propagation direction of the pump beam are collinear. As a result, no deflection in the LC laser beam is observed on the illumination screen (Figure 3c(ii)). By continuing the scanning from location I to V, the LC laser beam is translated in the opposite direction on the screen. In this case, the LC laser emission is found to occur at larger values of θ as the alignment of the substrate normal relative to the propagation direction of the pump beam increases. For example, at the location labelled as II (Figure 3c(iii)), the LC laser is deflected by an angle of $\theta = 12^\circ$ which increases to values of θ of 24° , 36° and 42° , as the pump beam is scanned through the active regions, III, IV, and V, respectively.

Adjusting the radius of curvature of the flexible laser enables the amount of beam steering to be controlled, i.e., a larger radius of curvature leads to shallower beam steering and vice-versa. In the illustration, the radius of curvature of the flexible device is 5 mm resulting in beam-steering of the LC laser of up to 42°. This feature means that the LC laser emission can be propagated in a range of directions without tilting the laser device. It should be noted that when the device is held in a curved configuration, there is the potential for a slight change in the film thickness at a given location, which can result in a small alteration in the laser emission wavelength in accordance with a shift in the defect-mode as observed in Figure S3.

In this study we have demonstrated a flexible and mechanically robust defect-mode laser that exhibits single-mode laser emission at 582 nm, with an excitation threshold of $12.3 \pm 0.5 \mu\text{J}/\text{cm}^2/\text{pulse}$ and a slope efficiency of $6.0 \pm 0.3\%$. Experimental results are presented for the emission characteristics of the device, which is validated by simulations carried out using the 4×4 Berreman matrix approach. By virtue of the flexibility of the device, beam steering is demonstrated by simply bending the device without the need for any additional optical components. The properties of this laser device are particularly attractive for conformable platforms and potentially wearable photonics technologies.

Experimental Section

Materials and Fabrication

For this study, the photo-polymerizable chiral nematic liquid crystal (CLC) mixture, RMS11-68 (obtained from Merck®) was used as the CLC films. The mixture has a clearing temperature of $T_c = 79 \pm 1^\circ\text{C}$, a pitch of ~ 385 nm and after photo-polymerization is found to exhibit a selective reflection band centered at $\lambda = 615 \pm 5$ nm. To prepare the polymerized film, the toluene solvent in which the CLC is dispersed was first evaporated by stirring the mixture at room temperature ($T = 25^\circ\text{C}$) for 40 hours at 200 rpm. After evaporation of the solvent, the

mixture was then injected at 79°C via capillary action into a glass cell that consisted of rubbed polyimide on the inner surfaces of the glass substrates and a nominal cell gap of 5 μm .

The cell was then thermally annealed to minimize the number and density of disclination line observed in the Grandjean texture of the chiral nematic phase by heating the sample to the clearing temperature on a hotplate and cooling slowly to room temperature. During the cooling process, the sample was gently rubbed along one direction until it reached room temperature to promote a uniform alignment of the helix axis of the CLC (helix axis parallel to the normal of the glass substrates). The thermal annealing and rubbing process was repeated twice and the device was left on a flat surface in dark conditions for up to 48 hours. The sample was then inspected on a BX51 optical polarizing microscope to confirm that the density of oily streaks was low with large area monodomains of the CLC texture. Following visual inspection, the sample was then photo-cured using an ultraviolet light ($\lambda = 365 \text{ nm}$) source (CS2010, Thorlabs) with a power density of $P = 14 \pm 2 \text{ mWcm}^{-2}$ for 40 seconds, which was measured using a power meter (PM100D, Thorlabs) attached to a photo-diode (S120VC, Thorlabs). All of the above steps were carried out in either yellow light or in dark conditions until the sample was fully crosslinked.

The device fabrication steps are illustrated in the Figure 1a. After photo-polymerization the CLC film (Figure 1a.i), the superstrate was delaminated from glass (Figure 1a. ii). A pressure-sensitive adhesive on flexible substrate (made of polyethylene terephthalate) was applied to the CLC film and gently rubbed in one direction (Figure 1a.iii). The flexible substrate was then slowly peeled-off resulting in a transfer of the polymerized CLC film from the glass substrate to the flexible substrate (Figure 1a.iv). The CLC film was found to have a thickness of $5.0 \pm 0.1 \mu\text{m}$.

A commercially available MicroChem[®] PMMA/anisole (4wt. % anisole) mixture was spin coated at 4000 rpm for 30 seconds onto the CLC film (Figure 1a.v) and the sample was then baked for 50 ± 5 min at 40°C to dry the solvent. This creates a barrier layer of PMMA of thickness 180 ± 10 nm on the CLC film^[37]. The role of the barrier layer was to prevent the diffusion of the dye to the CLC layers. For the defect-layer, the laser dye pyrromethene 597, PM597 (Exciton) (1wt. %) was dispersed into the PMMA/anisole mixture and stirred for 24 hours at 200 rpm at 25°C . The PM597 dye was chosen as it is known to exhibit a high quantum efficiency when used in band-edge LC lasers and can be optically-excited with the second-harmonic of an Nd:YAG laser^[33]. This dye-doped PMMA mixture was then spin-coated on top of the PMMA barrier layer at 4000 rpm 30 sec (Figure 1a.vi). The sample is again baked at 40°C for 50 ± 5 min to remove the residual solvent creating a dye-doped PMMA defect layer of thickness 180 ± 10 nm^[37]. At this stage, the stack now consists of flexible substrate/CLC film/PMMA/dye-doped PMMA and is shown in Figure 1A.vii. The stack is then cut in half resulting in two identical stacks, Figure 1a.viii, which are then combined to complete the full device stack. In doing so, the dye-doped PMMA layer thickness, including barrier layers, becomes 720 ± 20 nm (Figure 1a.ix). The two stacks are glued together and the complete flexible device is shown in Figure 1a.x.

Simulation

The 4×4 Berreman matrix method is used to model the transmission spectrum of the complete device stack. The inputs to the model were the thickness of the CLC layers ($5 \mu\text{m}$, $n_o = 1.58$, $n_e = 1.71$, where n_e and n_o are the extraordinary and ordinary refractive indices), $0.18 \mu\text{m}$ -thickness for each barrier layer ($n = 1.50$) and $0.36 \mu\text{m}$ -thick PMMA defect-layer ($n = 1.50$). By adjusting the products $n_e p$ and $n_o p$, so that the edges of the transmission band coincide with those obtained from measurements, a defect-mode is observed to occur at 582 nm , which is consistent with our results for the laser emission wavelength.

Characterization of the Laser Emission

To observe defect-mode laser emission, the flexible device was optically pumped by an Nd:YAG laser (CryLas) that emitted short-pulses (1.4 ns) at the second harmonic ($\lambda_{\text{ex}} = 532$ nm). In this case, the repetition rate of the laser was set to 10 Hz to avoid bleaching of the laser dye. A neutral density filter wheel was used to adjust the pump energy. The pump beam was focused onto the flexible device using a 25 mm lens with the spot size 32.8 μm and the emission from the LC laser was then collected by a microscope objective and a focusing lens before it was directed to either an optical fiber that was connected to an Ocean optics USB 2000+ spectrometer. A long pass filter was inserted between the objective lens and the fiber to prevent the pump laser beam being detected. An illustration of the arrangement of the optical setup is provided in the Supporting Information, **Figure S1**.

In order to verify the polarization of the laser device, two CLC test samples with opposite handedness were prepared using the nematic host HTW114200-100 (obtained from Fusol) and chiral dopants. The left-handed chiral dopant S811 (25 wt. %) was doped into the nematic host to form the left-handed test CLC while the right-handed chiral dopant R811 (25 wt. %) was used for the right-handed test CLC. The concentration of the chiral dopants was chosen so that the reflection band overlapped the LC laser emission wavelength ($\lambda_{\text{LC}} = 582$ nm). These test samples were inserted separately in between the flexible laser device and the collection optics, as shown in **Figure S4** to test the polarization state of the LC laser.

Supporting Information

Supporting Information is available from the Wiley Online Library or from the author.

Acknowledgements

T.A. thanks the Punjab Educational Endowment Fund (Pakistan) and the Vicky Noon Education foundation for financial support during his graduate studies. The authors thank Dr Owain Parri (Merck) for the supply of the polymerized CLC materials.

Received: ((will be filled in by the editorial staff))

Revised: ((will be filled in by the editorial staff))

Published online: ((will be filled in by the editorial staff))

References

- [1] W. Zhang, J. Yao, Y. S. Zhao, *Acc. Chem. Res.* **2016**, *49*, 1691.
- [2] I. D. W. Samuel, G. A. Turnbull, *Chem. Rev.* **2007**, *107*, 1272.
- [3] H. Finkelmann, S. T. Kim, A. Muñoz, P. Palffy-Muhoray, B. Taheri, *Adv. Mater.* **2001**, *13*, 1069.
- [4] P. V. Shibaev, J. Madsen, A. Z. Genack, *Chem. Mater.* **2004**, *16*, 1397.
- [5] A. Varanytsia, H. Nagai, K. Urayama, P. Palffy-Muhoray, *Sci. Rep.* **2015**, *5*, 17739.
- [6] T. Matsui, R. Ozaki, K. Funamoto, M. Ozaki, K. Yoshino, *Appl. Phys. Lett.* **2002**, *81*, 3741.
- [7] S. M. Wood, F. Castles, S. J. Elston, S. M. Morris, *RSC Adv.* **2016**, *6*, 31919.
- [8] O. Painter, *Science (80-.)*. **1999**, *284*, 1819.
- [9] K. Zhong, L. Liu, X. Xu, M. Hillen, A. Yamada, X. Zhou, N. Verellen, K. Song, S. Van Cleuvenbergen, R. Vallée, K. Clays, *ACS Photonics* **2016**, *3*, 2330.
- [10] M. Li, X. Lai, C. Li, Y. Song, *Mater. Today Nano* **2019**, *6*, 100039.
- [11] W. Zhou, S.-C. Liu, X. Ge, D. Zhao, H. Yang, C. Reuterskiold-Hedlund, M. Hammar, *IEEE J. Sel. Top. Quantum Electron.* **2019**, *25*, 1.
- [12] J.-C. Huang, Y.-C. Hsiao, Y.-T. Lin, C.-R. Lee, W. Lee, *Sci. Rep.* **2016**, *6*, 28363.
- [13] J. Yoon, W. Lee, J. M. Caruge, M. Bawendi, E. L. Thomas, S. Kooi, P. N. Prasad, *Appl. Phys. Lett.* **2006**, *88*, 10.
- [14] H. de Vries, *Acta Crystallogr.* **1951**, *4*, 219.
- [15] Y. S. Liu, H. C. Lin, H. L. Xu, *IEEE Photonics J.* **2018**, *10*, 1.
- [16] I. P. Ilchishin, E. A. Tikhonov, T. V. Mykytiuk, *Mol. Cryst. Liq. Cryst.* **2018**, *670*, 112.
- [17] A. H. Gevorgyan, K. B. Oganessian, *Laser Phys. Lett.* **2015**, *12*, 125805.

- [18] J. Schmidtke, W. Stille, *Eur. Phys. J. B - Condens. Matter* **2003**, *31*, 179.
- [19] J. Schmidtke, W. Stille, H. Finkelmann, *Phys. Rev. Lett.* **2003**, *90*, 083902.
- [20] V. I. Kopp, B. Fan, H. K. M. Vithana, A. Z. Genack, *Opt. Lett.* **1998**, *23*, 1707.
- [21] J. Schmidtke, W. Stille, *Eur. Phys. J. E* **2003**, *12*, 553.
- [22] I. P. Ilchishin, E. A. Tikhonov, T. V. Mykytiuk, *Mol. Cryst. Liq. Cryst.* **2016**, *639*, 47.
- [23] M. H. Song, B. Park, K.-C. Shin, T. Ohta, Y. Tsunoda, H. Hoshi, Y. Takanishi, K. Ishikawa, J. Watanabe, S. Nishimura, T. Toyooka, Z. Zhu, T. M. Swager, H. Takezoe, *Adv. Mater.* **2004**, *16*, 779.
- [24] H. Yoshida, C. H. Lee, Y. Matsuhisa, A. Fujii, M. Ozaki, *Adv. Mater.* **2007**, *19*, 1187.
- [25] S. M. Jeong, N. Y. Ha, Y. Takanishi, K. Ishikawa, H. Takezoe, S. Nishimura, G. Suzuki, *Appl. Phys. Lett.* **2007**, *90*, 261108.
- [26] M. Ozaki, R. Ozaki, T. Matsui, K. Yoshino, *Jpn. J. Appl. Phys.* **2003**, *42*, L472.
- [27] M. Uchimura, Y. Watanabe, F. Araoka, J. Watanabe, H. Takezoe, G. Konishi, *Adv. Mater.* **2010**, *22*, 4473.
- [28] M. C. Normand, P. Chen, C. Can, P. J. W. Hands, *Opt. Express* **2018**, *26*, 26544.
- [29] Y. Watanabe, M. Uchimura, F. Araoka, G. Konishi, J. Watanabe, H. Takezoe, *Appl. Phys. Express* **2009**, *2*, 102501.
- [30] A. J. C. Kuehne, M. C. Gather, *Chem. Rev.* **2016**, *116*, 12823.
- [31] Y. Inoue, H. Yoshida, K. Inoue, A. Fujii, M. Ozaki, *Appl. Phys. Express* **2010**, *3*, 102702.
- [32] H. Coles, S. Morris, *Nat. Photonics* **2010**, *4*, 676.
- [33] C. Mowatt, S. M. Morris, M. H. Song, T. D. Wilkinson, R. H. Friend, H. J. Coles, *J. Appl. Phys.* **2010**, *107*, 043101.
- [34] S. Gao, Y. Zhai, X. Zhang, X. Song, J. Wang, I. Drevensek-Olenik, R. Rupp, J. Xu, *Polymers (Basel)*. **2018**, *10*, 805.
- [35] J. E. Stockley, G. D. Sharp, K. M. Johnson, *Opt. Lett.* **1999**, *24*, 55.

- [36] Y.-C. Yang, C.-S. Kee, J.-E. Kim, H. Y. Park, J.-C. Lee, Y.-J. Jeon, *Phys. Rev. E* **1999**, *60*, 6852.
- [37] MicroChem Corp., PMMA Electron-Beam resist.

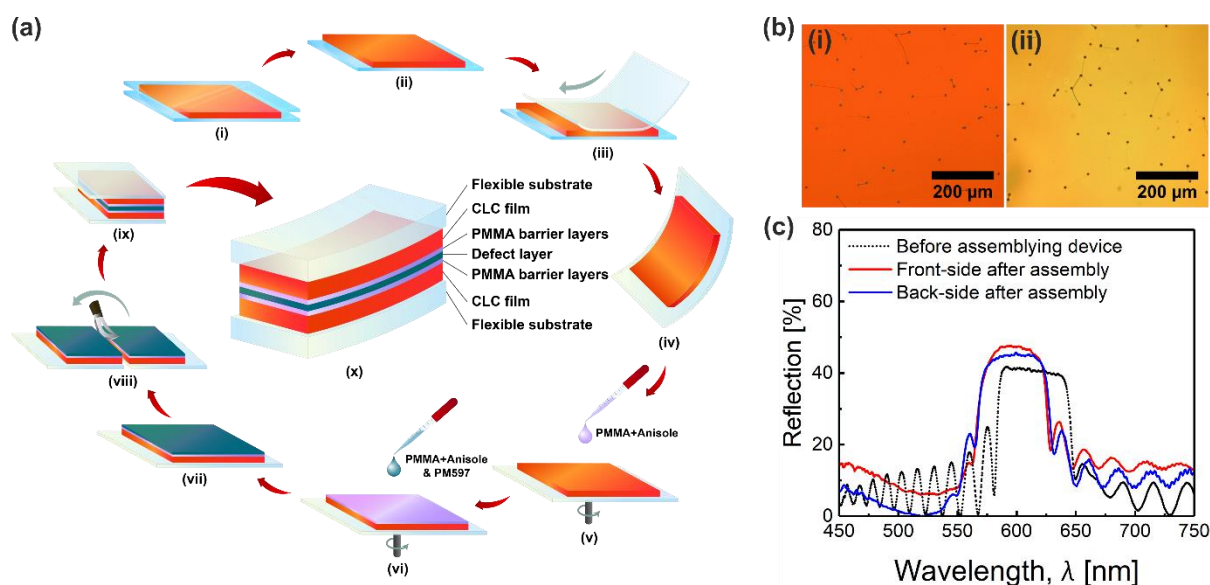


Figure 1. (a) Illustration of the fabrication process used to construct the flexible LC defect-mode laser, **(i)** mixture injection and photo-polymerization to form the CLC film, **(ii)** removal of the top glass substrate, **(iii)** film transfer to flexible substrate **(iv)** CLC film on a flexible substrate, **(v)** spin-coating of the PMMA barrier layer, **(vi)** spin-coating of the dye-doped PMMA (defect) layer, **(vii)** single stack, **(viii)** separation of CLC into top and bottom layers, **(ix)** combing the stacks, and **(x)** the complete device stack. **(b)** Optical polarization microscope images (viewed in reflection) of the photo-polymerized CLC film **(i)** before transfer to the flexible substrate and **(ii)** after assembling the flexible laser device. **(c)** Reflection spectra of the photo-polymerized CLC film before transfer onto the flexible substrate (black line) and after assembling the full device stack (red line – reflection from top CLC, blue line – reflection from the bottom CLC layer).

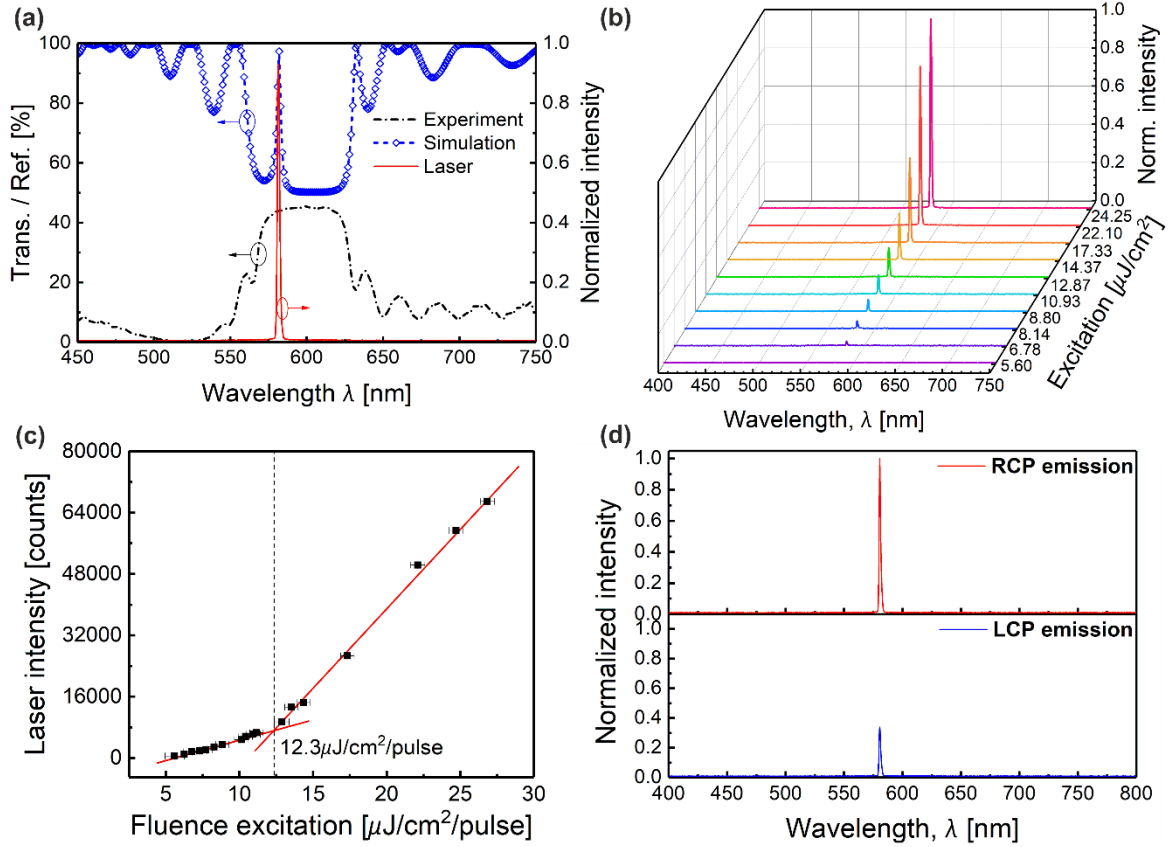


Figure 2. (a) Reflection spectrum of the band-gap (black line, primary axis) of the full flexible device, (blue line, primary axis) 4×4 Berreman simulation showing the transmission spectrum for the device stack with a transmission notch at 582 nm (parameters for the simulation are described in the Experimental Section), (red line, secondary axis) laser emission spectrum for the flexible device when optically excited with nanosecond pulses from an Nd:YAG laser at $\lambda_{\text{exc}} = 532$ nm. The emission wavelength is found to be centered at 582 nm with a linewidth of 1.97 nm. (b) laser emission spectrum as a function of the excitation energy, (c) peak laser intensity as a function of the excitation fluence showing an excitation threshold of $12.3 \mu\text{J}/\text{cm}^2/\text{pulse}$, and (d) laser emission spectra for the right circularly polarized component (red line) and left circularly polarized component (blue line) of the laser emission.

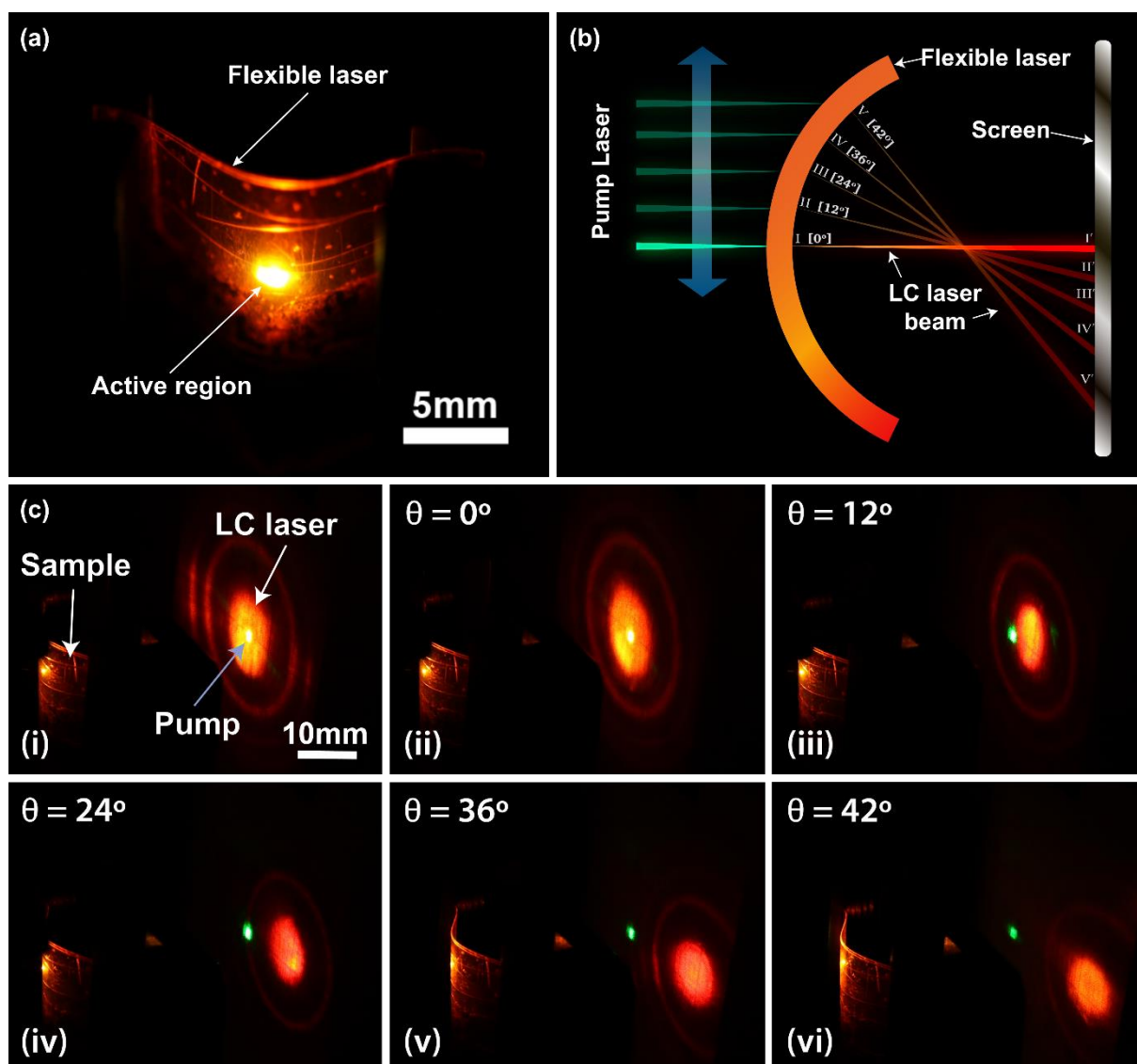


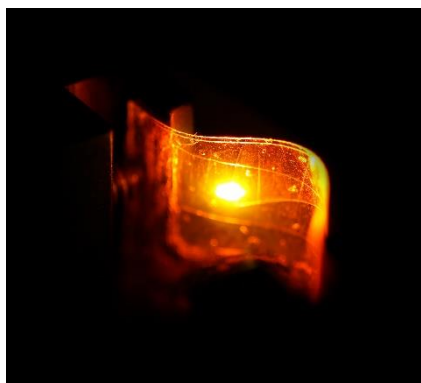
Figure 3. (a) Photograph of the flexible laser device when subjected to a mechanically-induced deformation and optically excited with an Nd:YAG laser, (b) a diagram illustrating the beam steering concept when the flexible laser is deformed and the pump beam from the Nd:YAG laser is scanned across the device. (c) (i) Photograph showing the flexible laser, the pump beam and the LC laser emission observed on the white illumination screen. (ii - vi) Photographs demonstrating the steering of the LC laser beam as the pump beam is scanned across the curved flexible laser device.

A flexible defect-mode liquid crystal laser is demonstrated that has been fabricated using a facile and cost-effective film transfer technique. The laser exhibits a low threshold fluence of $12.3 \pm 0.5 \mu\text{J}/\text{cm}^2/\text{pulse}$. Beam steering is observed when the device is subjected to a mechanical deformation, which shows potential for wearable and flexible technologies.

Keyword *thin film laser, liquid crystal, defect-mode, flexible laser*

Taimoor Ali, Jia-De Lin, Benjamin Snow, Xiuze Wang, Steve J. Elston and Stephen M. Morris**

A Thin-Film Flexible Defect-Mode Laser



Supporting Information

A Thin-Film Flexible Defect-Mode Laser

*Taimoor Ali**, *Jia-De Lin*, *Benjamin Snow*, *Xiuze Wang*, *Steve J. Elston* and *Stephen M. Morris**

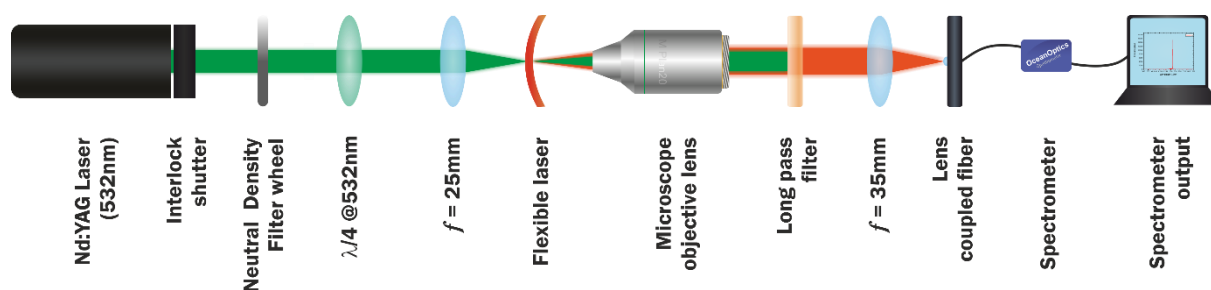


Figure S1: Free space optical arrangement used to excite the flexible laser device using an Nd:YAG ($\lambda_{\text{exc}} = 532\text{nm}$) pulsed laser with a 10 Hz repetition rate.

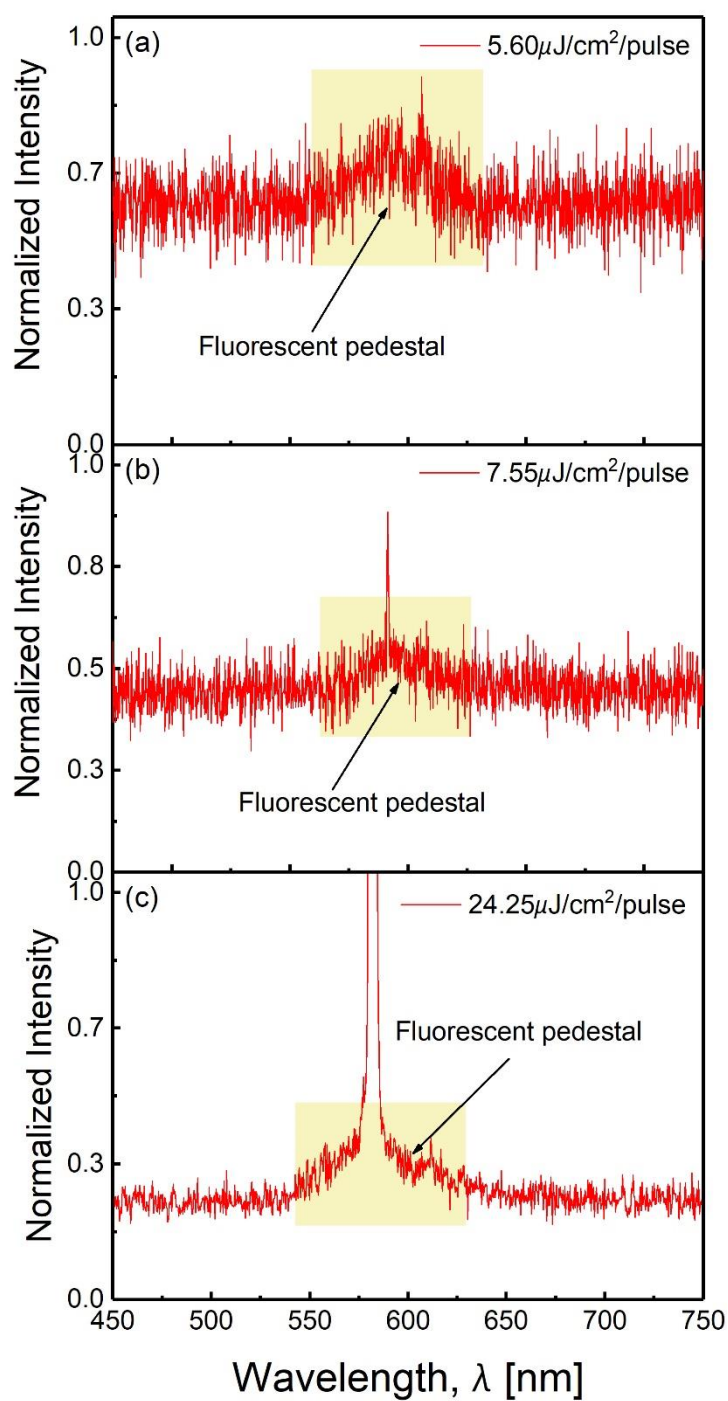


Figure S2: The fluorescent pedestal from the flexible laser when pumped the Nd:YAG laser at different excitation fluence. The fluorescent pedestal centered at the 585 nm with excitation fluence (a) 5.6 $\mu\text{J}/\text{cm}^2/\text{pulse}$, (b) 7.55 $\mu\text{J}/\text{cm}^2/\text{pulse}$, and (c) 24.25 $\mu\text{J}/\text{cm}^2/\text{pulse}$.

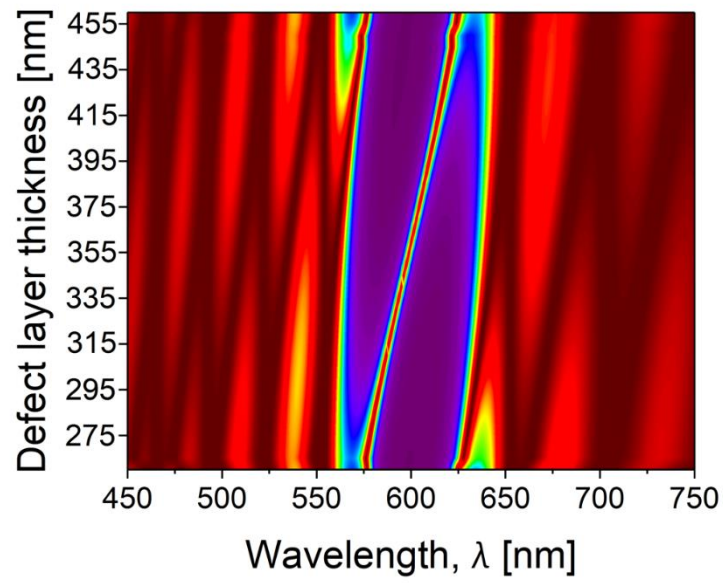


Figure S3: 4×4 Berreman simulations to demonstrate that the position of the defect-mode can be controlled by varying the thickness of the defect layer. In the model, the defect thickness is varied from 260 nm to 460 nm resulting in a leaky (defect) mode that varies from 575 nm to 625 nm, respectively. The model parameters are $p = 365\text{nm}$, $n_o = 1.58$ and $n_e = 1.71$.

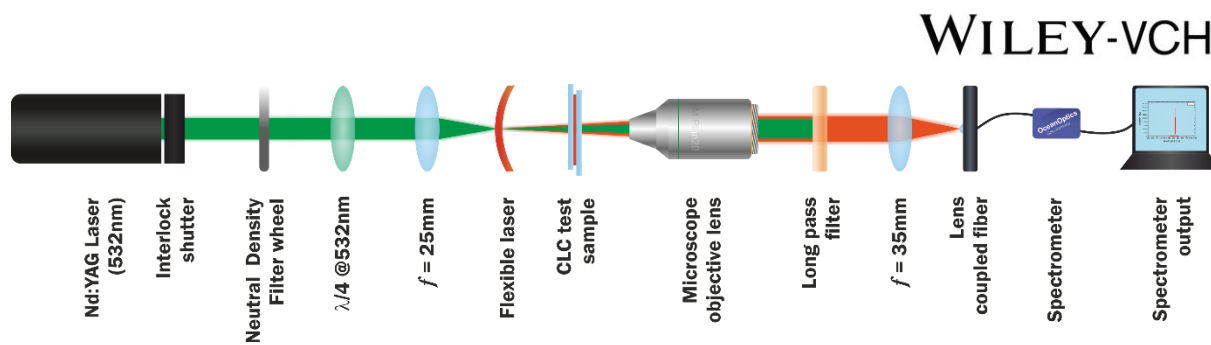


Figure S4: Experimental configuration used to determine the polarization state of the LC laser emission by using CLC test samples of known handedness. The test samples were inserted in between the flexible laser and the microscope objective lens.